NASA Technical Memorandum 84237

NASA-TM-84237 19820015363

Validation of Zero-Order Feedback Strategies for Medium-Range Air-to-Air Interception in a Horizontal Plane

Josef Shinar

April 1982

National Aeronautics and
Space Administration

NASA Technical Memorandum 84237

Validation of Zero-Order Feedback Strategies for Medium-Range Air-to-Air Interception in a Horizontal Plane

Josef Shinar, Ames Research Center, Moffett Field, California

National Aeronautics and
Space Administration

Ames Research Center
Moffett Field, California 94035

TABLE OF CONTENTS

LIST OF TABLES

LIST OF FIGURES

SYMBOLS

a	speed of sound
C_D	total drag coefficient
C_{D0}	zero-lift drag coefficient
C_L	lift coefficient
C_{L_1}	lift coefficient for level flight
D	total aerodynamic drag force
D_0	zero-lift drag force
D_i	induced-drag force in level flight
d	distance of capture
e	evader strategy
g	acceleration of gravity
h	altitude
$\mathscr{H}$	Hamiltonian function
$\mathscr{J}$	cost function of the game
K	induced-drag parameter
L	aerodynamic lift force
M	Mach number
n	aerodynamic load factor defined by equation (18)
P	atmospheric pressure
p	pursuer strategy
q	dynamic pressure defined by equation (15)
R	distance of separation (range)
r	best turning radius at a given speed
S	aircraft wing surface
T	thrust force
t	time

U	functional form of u
u	normalized turning-control function
V	velocity
W	aircraft weight
$\left(\frac{W}{S}\right)$	aircraft wing loading
X, Y	Cartesian coordinates
β	angular error defined in figure 3
ϵ	singular perturbation parameter
ϵ_g	geometrical perturbation parameter defined in equation (166)
λ_M	Mach number adjoint
λ_R	range adjoint
λ_χ	turning adjoint
λ_ψ	line-of-sight adjoint
Λ_M	functional form of λ_M
Λ_χ	functional form of λ_χ
μ	aircraft bank angle
ξ	throttle control parameter
ρ	air density
τ	stretched time scale
χ	aircraft flying direction (azimuth)
ψ	line-of-sight angle, defined in figure 1

Subscripts:

c	value at the corner velocity as defined by equation (30)
E	evader
f	final value
min	minimal value
max	maximal value
P	pursuer
s	sustained
0	initial value

Superscripts:

c	composite zero-order solution
i	inner-boundary-layer solution
o	outer-boundary-layer solution
r	reduced-order solution
*	optimal value
$(\bar{\ })$	nondimensional variable
$(\ )'$	derivation with respect to normalized time
$(\dot{\ })$	derivation with respect to real time
$(\hat{\ })$	distances divided by the speed of sound (refs. 17-19)

VALIDATION OF ZERO-ORDER FEEDBACK STRATEGIES FOR MEDIUM-RANGE AIR-TO-AIR INTERCEPTION IN A HORIZONTAL PLANE

Josef Shinar*

NASA Ames Research Center

SUMMARY

A zero-order feedback solution of a variable-speed interception game between two aircraft in the horizontal plane, obtained by using the method of forced singular perturbations (FSP), is compared with the exact open-loop solution. The comparison indicates that for initial distances of separation larger than 8 turning radii of the evader, the accuracy of the feedback approximation is better than 1%. The result validates the zero-order FSP approximation for medium-range air-combat analysis. This feedback solution is a very attractive candidate for airborne implementation.

1. INTRODUCTION

There is little doubt that the differential game approach is the most realistic mathematical formulation for air-to-air combat problems. As pointed out in a recent review paper by Ardema (ref. 1), however, "...this approach is so complex that results to date have been disappointing." Some hope for a relative breakthrough in this area has arisen with the application of singular-perturbation techniques for nonlinear zero-sum pursuit-evasion games (refs. 2-6). This method has created the potential to generate approximate feedback strategies for an important class of air-combat problems, namely, for medium-range air-to-air interception. (Generally, interception ranges are characterized by the firing envelope of the respective weapon systems. In this context "medium range" is a loose term covering a domain of weapon delivery between 4-20 km, excluding both long-range missiles, such as the AIM-54 Phoenix, and guns or other short-range weapons.)

The approximate solution obtained by the method of singular perturbations seems to be a very attractive candidate for airborne implementation. The practical usefulness of the approximation has to be evaluated not only by its feasibility, but more importantly by its accuracy. For accuracy assessment of any approximation the knowledge of the exact solution is required. In the last decade, several numerical algorithms were developed to solve the multidimensional, nonlinear, two-point boundary-value problem formulated by the set of necessary conditions of game optimality (refs. 7-14). Even if it is virtually impossible to prove that the converged numerical solution of the necessary conditions is indeed optimal, that is, that it satisfies the sufficiency conditions for saddle-point optimality (ref. 15), the only available way to assess the accuracy of an approximation is by comparing it with an outcome of some iterative computing algorithm. Unfortunately, most of the computer programs (refs. 7-12) are inoperative. The presently active computing algorithms (refs. 13-14) were also unable to provide the required comparison. Communication

*Senior NRC Associate on sabbatical leave from Technion, Israel Institute of Technology, Haifa, Israel.

with the research personnel involved revealed that the algorithms are currently limited to the solution of fixed-time problems. Moreover, there is a major problem of convergence for the relatively long duration of a medium-range interception (ref. 16).

Lately, another opportunity has appeared for validating the zero-order feedback approximation obtained by using singular-perturbation methods. An open-loop solution of the variable-speed aircraft versus aircraft pursuit-evasion game in a horizontal plane was published in several recent papers (refs. 17-19). This research effort is continuing at Ames Research Center. The open-loop solution method allows a relatively detailed comparison with a feedback approximation of the same problem, using an identical aero-propulsive model. The comparison has been limited to the already existing numerical results.

The objective of this paper is to report the outcome of the above described comparison and to draw appropriate conclusions. In section 2 the medium-range air-to-air interception game in a horizontal plane is formulated and the necessary conditions for saddle-point optimality are summarized. In section 3 the zero-order feedback solution of the game is developed, using the technique of forced singular perturbation, summarizing the approach detailed in references 2-5. In section 4 the basic concept of the open-loop solution (refs. 17-19) is described, and in section 5 the conditions of the comparison and the aerodynamic and propulsion models are detailed. Results of the comparison are presented and discussed in section 6 and the conclusions are drawn in section 7.

2. FORMULATION OF THE AIR-TO-AIR INTERCEPTION IN THE HORIZONTAL PLANE

2.1 Equations of Motion

The geometry of the relative position of two airplanes in a horizontal plane is depicted in figure 1. In an interception scenario, one airplane (having a superior weapons system) is the pursuer P, and the other is the evader E. The dynamics of the relative geometry can be expressed either in polar coordinates,

$$\dot{R} = -V_P \cos(\chi_P - \psi) + V_E \cos(\chi_E - \psi); \quad R(t_0) = R_0 \tag{1}$$

$$\dot{\psi} = [-V_P \sin(\chi_P - \psi) + V_E \sin(\chi_E - \psi)]/R; \quad \psi(t_0) = \psi_0 \tag{2}$$

or in a Cartesian coordinate system,

$$\dot{X} = V_E \cos\chi_E - V_P \cos\chi_P \; ; \quad X(t_0) = X_0 \tag{3}$$

$$\dot{Y} = V_E \sin\chi_E - V_P \sin\chi_P \; ; \quad Y(t_0) = Y_0 \tag{4}$$

by defining

$$X = X_E - X_P \tag{5}$$

$$Y = Y_E - Y_E \tag{6}$$

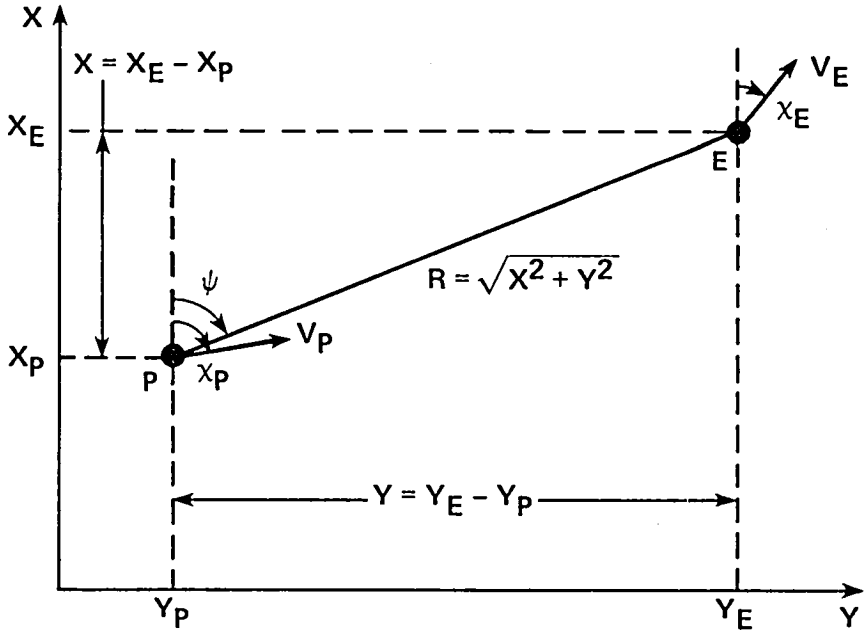

Figure 1.- Geometry of horizontal interception.

Aircraft dynamics for trajectory computations can be adequately represented by a point-mass approximation. In most studies (refs. 3-6, 17-24), constant weight and thrust aligned with the velocity vector are also assumed. This set of assumptions leads to

$$\dot{V}_P = g\left(\frac{T}{W} - \frac{D}{W}\right)_P = g(\bar{T}_P - \bar{D}_P) \quad ; \quad V_P(t_0) = V_{P_0} \tag{7}$$

$$\dot{V}_E = g\left(\frac{T}{W} - \frac{D}{W}\right)_E = g(\bar{T}_E - \bar{D}_E) \quad ; \quad V_E(t_0) = V_{E_0} \tag{8}$$

$$\dot{\chi}_P = \left(\frac{g}{V_P}\right) \text{tg } \mu_P = \left(\frac{g}{V_P}\right)\left[\left(\frac{L}{W}\right)_P^2 - 1\right]^{1/2} \quad ; \quad \chi_P(t_0) = \chi_{P_0} \tag{9}$$

$$\dot{\chi}_E = \left(\frac{g}{V_E}\right) \text{tg } \mu_E = \left(\frac{g}{V_E}\right)\left[\left(\frac{L}{W}\right)_E^2 - 1\right]^{1/2} \quad ; \quad \chi_E(t_0) = \chi_{E_0} \tag{10}$$

The normalized propulsive thrust and the aerodynamic lift and drag forces can be expressed by

$$\frac{T}{W} \triangleq \bar{T} = \xi \, \bar{T}_{max}(h,M) \tag{11}$$

$$\frac{L}{W} \triangleq n = q(h,M) \; C_L / \left(\frac{W}{S}\right) \tag{12}$$

$$\frac{D}{W} = \bar{D} = q(h,M) \; C_D(C_{L_1}M) / \left(\frac{W}{S}\right) \tag{13}$$

where ξ is the throttle parameter in the range of

$$0 \leq \xi \leq 1 \tag{14}$$

where q is the dynamic pressure defined by

$$q(h,M) = \frac{1}{2} \rho(h) \; V^2 = 0.7 \; P(h) \; M^2 \tag{15}$$

and where the relationship between drag and lift is approximated by a parabolic polar

$$C_D(C_L,M) = C_{D_0}(M) + K(M) \; C_L^2 \tag{16}$$

The maximum admissible value of the lift coefficient is limited by aerodynamic phenomena (e.g., stall, buffetting, or instability):

$$C_L \leq C_{L_{max}}(M) \tag{17}$$

The total lift force is also limited because of structural constraints. This limitation is usually expressed via the aerodynamic load factor,

$$n \leq n_{max} \tag{18}$$

leading, for horizontal flight, to a bound of the aircraft bank angle:

$$|\mu| \leq \mu_{max} = \cos^{-1}\left\{\frac{1}{n_{max}}\right\} \tag{19}$$

By combining equations (12), (13), (16), and (17), the total drag-to-weight ratio can be expressed by

$$\bar{D} = \bar{D}_0 + n^2 \bar{D}_i \tag{20}$$

$\bar{D}_0$ being the zero lift drag and $\bar{D}_i$ the induced drag for level flight (n = 1) divided by aircraft weight:

$$\bar{D}_0 = C_{D_0}(M)\ q/\left(\frac{W}{S}\right) \tag{21}$$

$$\bar{D}_i = K(M)\ \left(\frac{W}{S}\right)/q \tag{22}$$

The nondimensional quantity $\left(\frac{W}{S}\right)/q$ is the lift coefficient for level flight,

$$\left(\frac{W}{S}\right)/q \triangleq C_{L_1}(h,M) \tag{23}$$

For a horizontal flight, where the speed of sound remains constant, it is convenient to replace the velocity as a state variable by the Mach number. Accordingly, the set of equations (1)-(10) can be rewritten in a nondimensional form, using equations (18)-(23), as well as a normalized time scale

$$\bar{t} = \left(\frac{g}{a}\right)[t - t_0] \tag{24}$$

and, ( )', denoting derivations with respect to nondimensional time:

$$M_P' = \bar{T}_P - (\bar{D}_0)_P - n_P^2(\bar{D}_i)_P \quad : \quad M_P(0) = M_{P_0} \tag{25}$$

$$M_E' = \bar{T}_E - (D_0)_E - n_E^2(D_i)_E \quad : \quad M_E(0) = M_{E_0} \tag{26}$$

$$\chi_P' = (n_P^2 - 1)^{1/2}/M_P = [\chi_P'(M_P)]_{max}\ u_P \quad ; \quad \chi_P(0) = \chi_{P_0} \tag{27}$$

$$\chi_E' = (n_E^2 - 1)^{1/2}/M_E = [\chi_E'(M_E)]_{max}\ u_E \quad ; \quad \chi_E(0) = \chi_{E_0} \tag{28}$$

Here, u_p, u_e are the normalized controls of the pursuer and the evader respectively, bounded by

$$|u_P| \leq 1 \quad ; \quad |u_E| \leq 1 \tag{29}$$

and the maximum turning rates are determined by the physical constraints (17) and (18). These constraints determine the region of instantaneous maneuverability

of the aircraft, as depicted in figure 2. Their intersection determines the so-called "corner velocity," or Mach number, M_c:

$$M_c = [n_{max}(\frac{W}{S})/0.7\ P(h)\ C_{L_{max}}(M_c)]^{1/2} \tag{30}$$

and the corresponding maximum instantaneous turning rate. At these flying conditions, the turning radius of the aircraft is minimal and is given by

$$r_c \triangleq V_c/\dot{\chi}_c = V_c^2/g(n_{max}^2-1)^{1/2} \tag{31}$$

Or using nondimensional variables,

$$\bar{r}_c \triangleq r_c\ g/a^2 = M_c^2/(n_{max}^2 - 1)^{1/2} \tag{32}$$

Substituting equation (30) into (32) and using equations (15) and (23) yields

$$\bar{r}_c = \frac{n_{max}}{(n_{max}^2 - 1)^{1/2}} \frac{C_{L_1}(M = 1)}{C_{L_{max}}(M_c)} \tag{33}$$

In figure 2 the line of best sustained turning rates, obtained equating maximum thrust and drag, is also shown:

$$\chi_s' = (n_s^2 - 1)^{1/2}/M \tag{34}$$

where the sustained load factor is given by

$$n_s = [(\bar{T}_{max} - \bar{D}_0)/\bar{D}_i]^{1/2} \tag{35}$$

Figure 2 also indicates the admissible region of Mach numbers in horizontal flight. The lower bound is a consequence of equation (17) with $n = 1$, while the maximum Mach number can be either "placard" limited (because of structural and aerothermodynamical considerations) or determined by the equilibrium in straight flight:

$$M_{min} \leq M \leq M_{max}$$

$$M_{min} = [C_{L_1}(M = 1)/C_{L_{max}}]^{1/2} \tag{36}$$

$$M_{max} = \min \left\{ M_{limit},\ \tilde{M} \triangleq \max_M \arg\ [\bar{T}_{max} = \bar{D}_0 + \bar{D}_i] \right\}$$

The relative trajectory equations can be also rewritten in nondimensional form in polar coordinates as

$$\bar{R}' = -M_P \cos(\chi_P - \psi) + M_E \cos(\chi_E - \psi) \quad ; \quad \bar{R}(0) = \bar{R}_0 \tag{37}$$

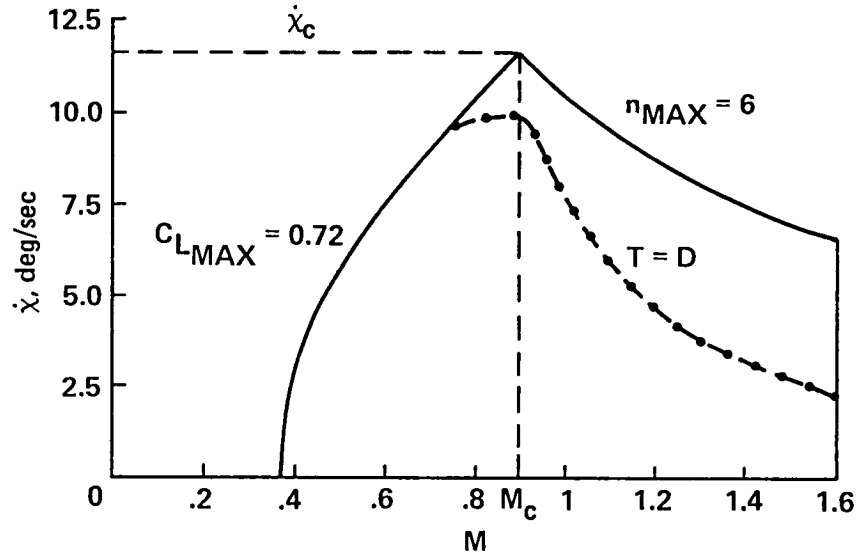

Figure 2.- Domain of maneuverability.

$$\psi' = [-M_P \sin(\chi_P - \psi) + M_E \sin(\chi_E - \psi)]/\bar{R} \quad ; \quad \psi(0) = \psi_0 \tag{38}$$

or in a Cartesian form as

$$\bar{X}' = M_E \cos\chi_E - M_P \cos\chi_P \quad ; \quad \bar{X}(0) = \bar{X}_0 \tag{39}$$

$$\bar{Y}' = M_E \sin\chi_E - M_P \sin\chi_E \quad ; \quad \bar{Y}(0) = \bar{Y}_0 \tag{40}$$

2.2 Differential Game Formulation

In this subsection an air-to-air interception engagement is formulated, based on the nondimensional mathematical model described previously, as a zero-sum differential game. For such a formulation the following elements have to be defined: game space; game dynamics; admissible control sets; role determination of the players; information structure; game termination; and cost function.

For the game dynamics described by equations (37), (38), and by (25)-(28), the six-dimensional game space ($\bar{R}$, ψ, M_P, M_E, X_P, X_E) is bounded by

$$\begin{aligned} 0 \leq \bar{R} &\leq \infty \\ (M_{min})_P \leq M_P &\leq (M_{max})_P \\ (M_{min})_E \leq M_E &\leq (M_{min})_E \end{aligned} \tag{41}$$

The angular state variables (ψ, χ_P, χ_E) are unbounded, but periodical; that is,

$$\begin{aligned} \psi + 2\pi &\equiv \psi \\ \psi_P + 2\pi &\equiv \chi_P \\ \chi_E + 2\pi &\equiv \chi_E \end{aligned} \tag{42}$$

The control set of the players is (ξ_P, u_P) and (ξ_E, u_E), respectively, subject to the constraints (14) and (29). The roles of the players (pursuer and evader) are determined at the outset by the superior weapons system of the interceptor airplane. This role determination remains unchanged during the duration of the game.

The game starts at some initial conditions ($\bar{R}_0$, ψ_0, M_{P_0}, M_{E_0}, χ_{P_0}, χ_{E_0}) at a moment ($t = 0$) when both players become aware of each other. For the duration of the game, perfect (memoryless) state information is assumed. The game terminates when the pursuer succeeds (at the first time) to approach the evader within a distance equal to the firing range of its weapon system. This condition is expressed by

$$\bar{R}(\bar{t}_f) = \bar{d} \tag{43}$$

$$\bar{R}'(\bar{t}_f) < 0 \tag{44}$$

The terminal values of the other state variables are free. Thus, equation (43) describes a five-dimensional terminal manifold, and equation (44) determines the "usable part" of this surface. The time of game termination (or in other words the "time of capture") is determined, based on equations (43)-(44), as

$$\bar{t}_f = \min_{\bar{t}} \arg\{\bar{R} = \bar{d}\} \qquad \bar{R}_o > \bar{d} \tag{45}$$

The cost function of the game is this time-of-capture,

$$\mathcal{J} = \bar{t}_f \tag{46}$$

The objective of the pursuer is to minimize $\bar{t}_f$; the evader wants (if capture cannot be avoided) to maximize $\bar{t}_f$.

The solution of this perfect information zero-sum differential game, for each set of initial conditions, is a triplet: a pair of optimal strategies $p^*(\cdot)$, $e^*(\cdot)$ and the saddle-point value of the cost function $\mathcal{J}^*$, satisfying.

$$\mathcal{J}(p, e^*) \geq \mathcal{J}(p^*, e^*) \triangleq \mathcal{J}^* \geq \mathcal{J}(p^*, e) \tag{47}$$

This quantitative game (game of degree) has a meaning only if capture, defined by equations (43) and (44), can be guaranteed. An obvious requirement for satisfying equation (44) even for a "tail-chase" configuration is

$$M_p(\bar{t}_f) > M_E(\bar{t}_f) \tag{48}$$

Analysis of a simplified constant-speed pursuit-evasion game indicates that capture can be achieved from any initial condition (ref. 20), even against an evader of unlimited maneuverability ($r_E = 0$), if the ratio of the "capture range," $\bar{R}(t_f) = \bar{d}$ to the pursuer turning radius r_P exceeds the value $[2(1 - \sin 1)]^{1/2}$; that is,

$$\bar{d}/\bar{r}_p > 0.563 \tag{49}$$

In interceptions where "all-aspect" guided missiles are used, this inequality is easily satisfied. It can be thus concluded that the medium-range interception engagement described in the Introduction is a suitable example for the above formulated differential game of degree. Such encounters are also characterized by an initial distance of separation $\bar{R}_0$ much larger than the firing range $\bar{d}$.

The first phase of the solution of such a differential game is to apply the set of necessary conditions for an assumed saddle-point optimality, generating a "candidate" for the solution. Then it has to be verified that the saddle-point inequality of equation (47) or some equivalent sufficiency condition (ref. 15) is indeed satisfied. For differential games of complex dynamic structure the verification phase is prohibitive; therefore, most investigations (refs. 7-14, 17-19) result only in "candidate" solutions.

2.3 Necessary Conditions of Optimality

The necessary conditions of saddle-point optimality for the previously formulated differential game are expressed by

$$\min_{\xi_P,\, u_P} \max_{\xi_E,\, u_E} \bar{\mathcal{H}}(\cdot) = 0 \tag{50}$$

The Hamiltonian of the normalized game is

$$\begin{aligned}\bar{\mathcal{H}} = 1 &+ \lambda_{\bar{R}}[-M_P \cos(\chi_P - \psi) + M_E \cos(\chi_E - \psi)] \\ &+ \lambda_\psi[-M_P \sin(\chi_P - \psi) + M_E \sin(\chi_E - \psi)]/\bar{R} \\ &+ \lambda_{M_P}[\xi_P(\bar{T}_{max})_P - (\bar{D}_0)_P - (\bar{D}_i)_P(1 + M_P^2(\chi'_{max})_P^2\, u_P^2)] \\ &+ \lambda_{M_E}[\xi_E(\bar{T}_{max})_E - (\bar{D}_0)_E - (\bar{D}_i)_E(1 + M_E^2(\chi'_{max})_E^2\, u_E^2)] \\ &+ \lambda_{\chi_P}(\chi'_{max})_P\, u_P + \lambda_{\chi_E}(\chi'_{max})_E\, u_E + \text{constraints}\end{aligned} \tag{51}$$

The multipliers $\lambda_{\bar{R}}$, etc., are the gradient components of the cost function $\mathcal{J}$ (assuming that such a gradient does exist) and they have to satisfy the set of adjoint differential equations:

$$\lambda_{\bar{R}}' = -\frac{\partial \bar{\mathcal{H}}}{\partial \bar{R}} \tag{52}$$

$$\lambda_\psi' = -\frac{\partial \bar{\mathcal{H}}}{\partial \Psi} \tag{53}$$

$$\lambda_{M_P}' = -\frac{\partial \bar{\mathcal{H}}}{\partial M_P} \tag{54}$$

$$\lambda_{M_E}' = -\frac{\partial \bar{\mathcal{H}}}{\partial M_E} \tag{55}$$

$$\lambda_{\chi_P}' = -\frac{\partial \bar{\mathcal{H}}}{\partial \chi_P} \tag{56}$$

$$\lambda_{\chi_E}' = -\frac{\partial \bar{\mathcal{H}}}{\partial \chi_E} \tag{57}$$

The end values of the adjoint variables are determined by the transversality conditions applied at the terminal manifold $\bar{R}(t_f) = \bar{d}$. Since all the other state variables are free on this surface,

$$\lambda\psi(\bar{t}_f) = \lambda_{M_P}(\bar{t}_f) = \lambda_{M_E}(\bar{t}_f) = \lambda_{\chi_P}(\bar{t}_f) = \lambda_{\chi_E}(\bar{t}_f) = 0 \tag{58}$$

By satisfying equations (50) and (44) at t_f, we also obtain

$$\lambda_{\bar{R}}(\bar{t}_f) = -1/\bar{R}'(t_f) = 1/[M_{P_f}\cos(\chi_{P_f} - \psi_f) - M_{E_f}\cos(\chi_{E_f} - \psi_f)] > 0 \tag{59}$$

The optimal control strategies can be obtained, in terms of the state and adjoint variables, by applying equation (50).

$$\xi_P^* = \frac{1}{2}[1 - \text{sign}\,\lambda_{M_P}] \quad , \quad \lambda_{M_P} \neq 0 \tag{60}$$

$$\xi_E^* = \frac{1}{2}[1 + \text{sign}\,\lambda_{M_E}] \quad , \quad \lambda_{M_E} \neq 0 \tag{61}$$

$$u_P^* = \text{sat}\,[(u_1^*)_P] \tag{62}$$

where $(u_1^*)_P$ is the unconstrained optimal turning strategy of the pursuer given by

$$(u_1^*)_P = \lambda_{\chi_P}/2\,\lambda_{M_P}(\bar{D}_i)_P\,M_P^2(\chi'_{max})_P \tag{63}$$

A similar expression holds for the evader.

It can be shown that a singular thrust subarc, requiring $\lambda'_{M_P} = \lambda_{M_P} = 0$ or $\lambda'_{M_E} = \lambda_E = 0$, is a candidate for this time-optimal game, only if $M_P = (M_{limit})_P$ or $M_E = (M_{limit})_E$, respectively. Equation (50) also requires that

$$\left.\frac{\partial^2 \mathcal{H}}{\partial u_P^2}\right|_{u_P = u_P^*} \geq 0 \tag{64}$$

$$\left.\frac{\partial^2 \mathcal{H}}{\partial u_E^2}\right|_{u_E = u_E^*} \leq 0 \tag{65}$$

These conditions imply, for unconstrained controls, that $\lambda_{M_P} < 0$ and $\lambda_{M_E} > 0$; that is, maximum thrust ($\xi^* = 1$) for both aircraft. Consequently, if zero thrust is optimal ($\xi^* = 0$) because of $\lambda_{M_P} > 0$ or $\lambda_{M_E} < 0$, it also requires that $u_P^* = \pm 1$ (or $u_E^* = \pm 1$). Conversely, constrained turning rate does not necessarily imply zero thrust.

To generate a candidate solution from some initial conditions of the game, a 12-dimensional nonlinear two-point boundary-value problem has to be solved. Several numerical techniques were developed to solve this problem (refs. 7-14), all requiring an excessive computational effort, impractical for a rapid systematical assessment, as well as for a real-time implementation. For such purposes an approximate analytical solution is preferred. Such an approximation can be obtained by the method of forced singular perturbations, as described in the next section.

3. ZERO-ORDER FEEDBACK SOLUTION

In this section an analytical approximation is outlined in order to provide a zero-order solution to the original differential game formulated in the preceding subsection. The approximation is based on applying the method of singular perturbations as described in references 2-6. First, a singularly perturbed dynamic model has to be defined. Analyzing this model to zero-order leads to a set of low-dimensional problems solvable analytically. Based on these simplified solutions, a uniformly valid zero-order approximation can be synthesized in a feedback form.

3.1 Modeling Considerations

The success of the singular-perturbation approach depends on the time-scale separation of the state variables. In this respect, inspection of the set of differential equations (37)-(38) and (25)-(28) leads to the following observations:

1. If the normalized separation distance $\bar{R}$ is sufficiently large, as assumed for a medium-range interception, the turning rate of the line of sight ψ', given by equation (38), will be very slow compared with the turning rates of the airplanes given in equations (27) and (28).

2. Longitudinal accelerations of an airplane (see eqs. (25) and (26)) are much smaller (of the order of ± 0.5 g or less) than the lateral accelerations (limited to 6-8 g) used for turning in equations (27) and (28).

3. Equations (32) and (38), describing the relative geometry in polar coordinates, are strongly connected and have to be analyzed on the same time scale.

Based on these observations the following hierarchy of state variables can be established: $\bar{R}$, ψ (slowest), M_P, M_E (faster), and χ_P, χ_E (fastest), leading to a singularly perturbed dynamic model. Such a model can be obtained either by proper rescaling of the variables, as in reference 2, or by artificial insertion of the perturbation parameter ϵ, as in references 3 and 4. It has been pointed out (ref. 5) that the second approach, called also a "forced" singular-perturbation technique (FSPT), leads to a zero-order solution which is identical to the result of scaling transformation. Because FSPT seems to be much more convenient for multiple time-scale problems, it is the approach used here.

The FSPT model of the differential game describing a medium-range air-to-air interception in nondimensional variables can be now formulated:

$$\bar{R}' = -M_P \cos(\chi_P - \psi) + M_E \cos(\chi_E - \psi) \qquad \bar{R}(0) = R_0 \tag{66}$$

$$\psi' = [-M_P \sin(\chi_P - \psi) + M_E \sin(\chi_E - \psi)]/\bar{R} \qquad \psi(0) = \psi_0 \tag{67}$$

$$\epsilon M_P' = \xi_P(\bar{T}_{max})_P - (\bar{D}_0)_P - (\bar{D}_i)_P [1 + M_P^2(\chi'_{max})_P^2 u_P^2] \qquad M_P(0) = M_{P_0} \tag{68}$$

$$\epsilon M_E' = \xi_E(\bar{T}_{max})_E - (\bar{D}_0)_E - (\bar{D}_i)_E [1 + M_E^2(\chi'_{max})_E^2 u_E^2] \qquad M_E(0) = M_{E_0} \tag{69}$$

$$\epsilon^2 \chi_P' = (\chi'_{max})_P u_P \qquad \chi_P(0) = \chi_{P_0} \tag{70}$$

$$\epsilon^2 \chi_E' = (\chi'_{max})_E u_E \qquad \chi_E(0) = \chi_{E_0} \tag{71}$$

The cost function $\mathcal{J}$ remains unchanged and the Hamiltonian of this singularly perturbed dynamic system becomes identical to the original one in equation (51) by setting for the adjoint variables of the FSPT model, denoted by a superscript "ϵ,"

$$\lambda^{\epsilon}_{M_P} = \epsilon \lambda_{M_P}, \; \lambda^{\epsilon}_{M_E} = \epsilon \lambda_{M_E}, \; \lambda^{\epsilon}_{\chi_P} = \epsilon^2 \lambda_{\chi_P}, \; \lambda^{\epsilon}_{\chi_E} = \epsilon^2 \lambda_{\chi_E} \tag{72}$$

This notation leads to the following set of adjoint differential equations, having a similar singularly perturbed structure as the state equations (66)-(71):

$$\lambda_{\bar{R}}' = -\frac{\partial \bar{\mathcal{H}}}{\partial \bar{R}} \qquad \lambda_{\bar{R}}(\bar{t}_f) > 0 \tag{73}$$

$$\lambda_{\psi}' = -\frac{\partial \bar{\mathcal{H}}}{\partial \psi} \qquad \lambda_{\psi}(\bar{t}_f) = 0 \tag{74}$$

$$\epsilon \lambda_{M_P}' = -\frac{\partial \bar{\mathcal{H}}}{\partial M_P} \qquad \lambda_{M_P}(\bar{t}_f) = 0 \tag{75}$$

$$\epsilon \lambda_{M_E}' = -\frac{\partial \bar{\mathcal{H}}}{\partial M_E} \qquad \lambda_{M_E}(\bar{t}_f) = 0 \tag{76}$$

$$\epsilon^2 \lambda_{\chi_P}' = -\frac{\partial \bar{\mathcal{H}}}{\partial \chi_P} \qquad \lambda_{\chi_P}(\bar{t}_f) = 0 \tag{77}$$

$$\epsilon^2 \lambda_{\chi_E}' = -\frac{\partial \bar{\mathcal{H}}}{\partial \chi_E} \qquad \lambda_{\chi_E}(\bar{t}_f) = 0 \tag{78}$$

When using this reformulation, the other necessary conditions of optimality — as equations (60)-(65), which were derived from equation (50) — remain unchanged.

The zero-order FSPT analysis consist of solving subsequently the following lower-dimensional problems: (1) a reduced-order game; (2) an outer boundary layer (velocity dynamics); and (3) an inner boundary layer (turning dynamics).

3.2 The Reduced-Order Game

Setting $\epsilon = 0$ in equations (60)-(71) and denoting the variables by a superscript "r" results in the following set of equations:

$$(\bar{R}^r)' = -M_P^r \cos(\chi_P^r - \psi^r) + M_E^r \cos(\chi_E^r - \psi^r) \qquad \bar{R}^r(0) = \bar{R}_0 \tag{79}$$

$$(\psi^r)' = [-M_P^r \sin(\chi_P^r - \psi^r) + M_E^r \sin(\chi_E^r - \psi^r)]/\bar{R}^r \qquad \psi^r(0) = \psi_0 \tag{80}$$

$$\xi_P^r(\bar{T}_{max})_P = (\bar{D}_0)_P + (\bar{D}_i)_P \tag{81}$$

$$\xi_E^r(\bar{T}_{max})_E = (\bar{D}_0)_E + (\bar{D}_i)_E \tag{82}$$

$$u_P^r = 0 \tag{83}$$

$$u_E^r = 0 \tag{84}$$

The Hamiltonian of the reduced game is

$$\bar{\mathcal{H}}^r = 1 + \lambda_{\bar{R}}^r [-M_P^r \cos(\chi_P^r - \psi^r) + M_E^r \cos(\chi_E^r - \psi^r)]$$

$$+ \lambda_\psi^r [-M_P^r \sin(\chi_P^r - \psi^r) + M_E^r \sin(\chi_E^r - \psi^r)]/\bar{R}^r + \text{constraints} \tag{85}$$

The constraints include now equations (81)-(84). Setting $\epsilon = 0$ in equations (73)-(78) as well, leads to

$$(\lambda_{\bar{R}}^r)' = -\frac{\partial \bar{\mathcal{H}}^r}{\partial \bar{R}^r} = (\lambda_\psi^r/\bar{R}^r)(\psi^r)' \quad ; \quad \lambda_{\bar{R}}^r(\bar{t}_f) > 0 \tag{86}$$

$$(\lambda_\psi^r)' = -\frac{\partial \bar{\mathcal{H}}^r}{\partial \psi^r} = \lambda_{\bar{R}}^r \bar{R}^r(\psi^r)' + (\lambda_\psi^r/\bar{R}^r)(\bar{R}^r)' \quad ; \quad \lambda_\psi^r(t_f) = 0 \tag{87}$$

$$-\frac{\partial \bar{\mathcal{H}}^r}{\partial M_P^r} = 0 \tag{88}$$

$$-\frac{\partial \bar{\mathcal{H}}^r}{\partial M_E^r} = 0 \tag{89}$$

$$-\frac{\partial \bar{\mathcal{H}}^r}{\partial \chi_P^r} = -M_P^r [\lambda_{\bar{R}}^r \sin(\chi_P^r - \psi^r) - \frac{\lambda_\psi^r}{\bar{R}^r} \cos(\chi_P^r - \psi^r)] = 0 \tag{90}$$

$$-\frac{\partial \bar{\mathcal{H}}^r}{\partial \chi_E^r} = -M_E^r [\lambda_{\bar{R}}^r \sin(\chi_E^r - \psi^r) - \frac{\lambda_\psi^r}{\bar{R}^r} \cos(\chi_E^r - \psi^r)] = 0 \tag{91}$$

The last four equations indicate that the "fast" variables M_P^r, M_E^r, χ_P^r, χ_E^r, have to be considered as additional control variables of the players constrained by equations (81)-(84). The last two equations lead to

$$\text{tg}(\chi_P^r - \psi^r) = \text{tg}(\chi_E^r - \psi^r) \triangleq \text{tg}\,\alpha^r = (\lambda_\psi^r/\bar{R}_r)/\lambda_{\bar{R}}^r \tag{92}$$

implying that

$$\alpha^r \triangleq (\chi_P^r - \psi^r) = (\chi_E^r - \psi^r) \pm m\pi \quad , \quad m = 0, 1 \ldots \tag{93}$$

Substituting (92) into (87) yields

$$(\lambda_\psi^r)' = (-M_P^r \pm M_E^r)\,[\lambda_{\underline{R}}^r \sin\alpha^r - (\lambda_\psi^r/\bar{R}^r)\cos\alpha^r] = 0 \tag{94}$$

and consequently

$$\lambda_\psi^r = \lambda_\psi(t_f) = 0 \tag{95}$$

leading to the conclusion that

$$\alpha^r = m_1\pi \quad ; \quad m_1 = 0, 1 \ldots \tag{96}$$

The correct values of the free ambiguity parameters m and m_1 can be determined from the saddle-point optimality of the reduced-order Hamiltonian. Substituting equation (95) into (85) and applying

$$\min_{M_P^r,\chi_P^r,\xi_P^r} \quad \max_{M_E^r,\chi_E^r,\xi_E^r} \quad \dot{\mathcal{H}}^r = 0 \tag{97}$$

leads, when combined with equation (67), to the following results

$$\chi_P^r = \chi_E^r = \psi^r = \psi_0 \tag{98}$$

Further application of equation (97), combined with equations (81) and (82), yields

$$M_P^r = (M_{max})_P \tag{99}$$

$$M_E^r = (M_{max})_E \tag{100}$$

$$\xi_P^r = [\bar{D}_0(M_{max})_P + \bar{D}_i(M_{max})_P]/\bar{T}_{max}(M_{max})_P \tag{101}$$

with a similar expression for the evader. Moreover, substitution of equations (98)-(100) into equations (85) and (97) leads to

$$\lambda_{\underline{R}}^r = \lambda_{\underline{R}}^r(\bar{t}_f) = 1/(M_P^r - M_E^r) \tag{102}$$

In summarizing all these results, it can be stated that the solution of the reduced-order game is a tail-chase flown by each airplane at its maximum speed. The optimal control strategies are given by equations (98)-(101). These strategies are playable (ref. 15) only if $(M_{max})_P > (M_{max})_E$, that is, if $\lambda_{\underline{R}}^r > 0$, as required by

equation (44). Since the reduced-order solution does not satisfy the initial conditions imposed on the fast variables (M_P, M_E, χ_P, χ_E) boundary-layer solutions are needed.

3.3 Zero-Order Outer Boundary Layer (Velocity Dynamics)

The first (outer) boundary layer is obtained by performing a time-stretching transformation

$$\tau^o = \bar{t}/\epsilon \tag{103}$$

on the equations (66)-(78) and setting again $\epsilon = 0$. This operation leads to the following equations, where the boundary layer variables are denoted by a superscript "o":

$$\frac{d\bar{R}^o}{d\tau^o} = 0 \quad \bar{R}^o = \bar{R}_0 \tag{104}$$

$$\frac{d\psi^o}{d\tau^o} = 0 \quad \psi^o = \psi_0 \tag{105}$$

$$\frac{dM_P^o}{d\tau^o} = \xi_P^o(\bar{T}_{max})_P - (\bar{D}_0)_P - (\bar{D}_i)_P \quad ; \quad M_P^o(0) = M_{P_0} \tag{106}$$

$$\frac{dM_E^o}{d\tau^o} = \xi_E^o(T_{max})_E - (\bar{D}_0)_E - (\bar{D}_i)_E \quad ; \quad M_E^o(0) = M_{E_0} \tag{107}$$

$$u_P^o = 0 \tag{108}$$

$$u_E^o = 0 \tag{109}$$

$$\frac{d\lambda_{\bar{R}}^o}{d\tau^o} = 0 \Rightarrow \lambda_{\bar{R}}^o(\tau^o) = \lambda_{\bar{R}}^r = 1/(M_P^r - M_E^r) \tag{110}$$

$$\frac{d\lambda_\psi^o}{d\tau^o} = 0 \Rightarrow \lambda_\psi^o(\tau^o) = \lambda_\psi^r = 0 \tag{111}$$

$$\frac{d\lambda_{M_P}^o}{d\tau^o} = -\frac{\partial \mathcal{H}^o}{\partial M_P^o} \quad ; \quad \lim_{\tau^o \to \infty} \lambda_{M_P}^o = \lambda_{M_P}(\bar{t}_f) = 0 \tag{112}$$

$$\frac{d\lambda_{M_E}^o}{d\tau^o} = -\frac{\partial \mathcal{H}^o}{\partial M_E^o} \quad ; \quad \lim_{\tau^o \to \infty} \lambda_{M_E}^o = \lambda_{M_E}(\bar{t}_f) = 0 \tag{113}$$

$$-\frac{\partial \mathcal{H}^o}{\partial \chi_P^o} = 0 \tag{114}$$

$$-\frac{\partial \mathcal{H}^o}{\partial \chi_E^o} = 0 \tag{115}$$

The Hamiltonian of this outer-boundary-layer game is

$$\mathcal{H}^o = 1 + \lambda_R^r [-M_P^o \cos(\chi_P^o - \psi_0) + M_E^o \cos(\chi_E^o - \psi_0)] + \lambda_{M_P}^o [\xi_P^o (\bar{T}_{max})_P$$

$$- (\bar{D}_0)_P - (\bar{D}_i)_P] + \lambda_{M_E}^o [\xi_E^o (\bar{T}_{max})_E - (\bar{D}_0)_E - (\bar{D}_i)_E)] + \text{constraints} \tag{116}$$

Game optimality requires

$$\min_{\xi_P^o,\ \chi_P^o} \max_{\xi_E^o,\ \chi_E^o} \mathcal{H}^o = 0 \tag{117}$$

yielding

$$\chi_P^o = \chi_E^o = \psi_0 \tag{118}$$

and

$$\xi_P^o = \frac{1}{2}[1 - \text{sign}\ \lambda_{M_P}^o] \qquad \lambda_{M_P}^o \neq 0 \tag{119}$$

$$\xi_E^o = \frac{1}{2}[1 - \text{sign}\ \lambda_{M_E}^o] \qquad \lambda_{M_E}^o \neq 0 \tag{120}$$

It is easily seen that this game can be decoupled into two independent optimization problems. It can be also shown that for each airplane there exists an equilibrium point determined by $M_P^o = (M_{max})_P$ or, respectively, $M_E^o = (M_{max})_E$, coinciding with the reduced-order solution. To reach these equilibrium points, which automatically satisfy the matching conditions, it is required (assuming $M_{P0} < (M_{max})_P$, $M_{E0} < (M_{max})_E$) that

$$\xi_P^o = \xi_E^o = 1 \tag{121}$$

The values of the adjoint variables $\lambda_{M_P}^o$ and $\lambda_{M_E}^o$ can be determined separately, by assuming that the opponent has already reached equilibrium, from equation (117), in a state feedback form:

$$\lambda_{M_P}^o = -\lambda_R^r [M_P^r - M_P^o]/[(\bar{T}_{max})_P - (\bar{D}_0)_P - (\bar{D}_i)_P] = -\Lambda_M(M_P^o) \tag{122}$$

$$\lambda_{M_E}^o = \lambda_R^r [M_E^r - M_E^o]/[(\bar{T}_{max})_E - (\bar{D}_0)_E - (\bar{D}_i)_E] = \Lambda_M(M_E^o) \tag{123}$$

It can be verified that equations (122) and (123) always satisfy equation (117) and that they are also compatible with equations (119)-(121). This outer boundary layer is therefore an accelerating straight-line "dash" for both airplanes in a tail-chase; that is, both velocity vectors are aligned with the line of sight. Since this direction does not satisfy the initial conditions χ_{P_0}, χ_{E_0} an additional boundary layer is required.

3.4 Zero-Order Inner Boundary Layer (Turning Dynamics)

In this second (inner) boundary layer a new stretching transformation

$$\tau^i = \bar{t}/\varepsilon^2 = \tau^o/\varepsilon \tag{124}$$

is used and the variables are indexed by a superscript "i." This transformation results, setting $\varepsilon = 0$, in the following:

$$\bar{R}^i = \bar{R}^o = \bar{R}^r = \bar{R}_0 \tag{125}$$

$$\psi^i = \psi^o = \psi^r = \psi_0 \tag{126}$$

$$M_P^i = M_P^o(\tau^o = 0) = M_{P_0} \tag{127}$$

$$M_E^i = M_E^o(\tau^o = 0) = M_{E_0} \tag{128}$$

$$\frac{d\chi_P^i}{d\tau^i} = [\chi_P'(M_{P_0})]_{max}\, u_P^i \quad ; \quad \chi_P^i(0) = \chi_{P_0} \tag{129}$$

$$\frac{d\chi_E^i}{d\tau^i} = [\chi_E'(M_{E_0})]_{max}\, u_E^i \quad ; \quad \chi_E^i(0) = \chi_{E_0} \tag{130}$$

$$\lambda_{\bar{R}}^i = \lambda_{\bar{R}}^o = \lambda_{\bar{R}}^r = 1/[M_P^r - M_E^r] \tag{131}$$

$$\lambda_\psi^i = \lambda_\psi^o = \lambda_\psi^r = 0 \tag{132}$$

$$\lambda_{M_P}^i = \lambda_{M_P}^o \tag{133}$$

$$\lambda_{M_E}^i = \lambda_{M_E}^o \tag{134}$$

$$\frac{d\lambda_{\chi_P}^i}{d\tau^i} = -\frac{\partial \mathcal{H}^i}{\partial \chi_P^i} \quad ; \quad \lim_{\tau^i \to \infty} \lambda_{\chi_P}^i = \lambda_{\chi_P}(\bar{t}_f) = 0 \tag{135}$$

$$\frac{d\lambda^i_{\chi_E}}{d\tau^i} = -\frac{\partial \mathcal{H}^i}{\partial \chi^i_E} \quad ; \quad \lim_{\tau^i \to \infty} \lambda^i_{\chi_E} = \lambda_{\chi_E}(\bar{t}_f) = 0 \tag{136}$$

where the Hamiltonian of this inner boundary layer is

$$\begin{aligned}\mathcal{H}^i = 1 &+ \lambda^r_{\bar{R}}\left[-M_{P_0}\cos(\chi^i_P - \psi_0) + M_{E_0}\cos(\chi^i_E - \psi_0)\right] \\ &+ \lambda^o_{M_P}\left\{\xi^i_P\,(\bar{T}_{max})_P - (\bar{D}_0)_P - (\bar{D}_i)_P\left[1 + M^2_{P_0}\,(\chi'_{max})^2_P\,u^{i^2}_P\right]\right\} \\ &+ \lambda^o_{M_E}\left\{\xi^i_E\,(\bar{T}_{max})_E - (\bar{D}_0)_E - (\bar{D}_i)_E\left[1 + M^2_{E_0}\,(\chi'_{max})^2_E\,u^{i^2}_E\right]\right\} \\ &+ \lambda^i_{\chi_P}\,(\chi'_{max})_P\,u^i_P + \lambda^i_{\chi_E}\,(\chi'_{max})_E\,u^i_E + \text{constraints}\end{aligned} \tag{137}$$

The necessary conditions of saddle-point optimality require

$$\min_{\xi^i_P,\,u^i_P} \max_{\xi^i_E,\,u^i_E} \mathcal{H}^i = 0 \tag{138}$$

leading to

$$\xi^i_P = \frac{1}{2}\left[1 - \text{sign}\,\lambda^o_{M_P}\right] = 1 \qquad \lambda^o_{M_P} \neq 0 \tag{139}$$

$$\xi^i_E = \frac{1}{2}\left[1 - \text{sign}\,\lambda^o_{M_E}\right] = 1 \qquad \lambda^o_{M_E} \neq 0 \tag{140}$$

$$u^i_P = \text{sat}\left[(u^i_l)_P\right] \tag{141}$$

$$u^i_E = \text{sat}\left[(u^i_l)_E\right] \tag{142}$$

with

$$(u^i_l)_P = \lambda\chi^i_P/2\lambda^o_{M_P}\,M^2_{P_0}(\bar{D}_i)_P(\chi'_{max})_P \tag{143}$$

$$(u^i_l)_E = \lambda\chi^i_E/2\lambda^o_{M_E}\,M^2_{E_0}(\bar{D}_i)_E(\chi'_{max})_E \tag{144}$$

From equations (129), (130), (135), (136), (143), and (144) the separability of the turning boundary-layer game into two independent optimal control problems can be concluded. Based on this independence, the inner boundary-layer adjoints can be eliminated from the Hamiltonian (138) assuming equilibrium of the opponent. Substituting equations (143) and (144) separately into equation (138), and using equations (122), (123), and (102) results in the following respective feedback expressions

$$(\lambda^i_{\chi_P})^2 = M_{P_0}^3(M_P^r - M_{P_0})[1 - \cos(\chi_P^i - \psi_0)]/(M_P^r - M_E^r)^2 = \Lambda_\chi^2(\chi_P^i, M_{P_0}, \psi_0) \quad (145)$$

$$(\lambda^i_{\chi_E})^2 = M_{E_0}^3(M_E^r - M_{E_0})[1 - \cos(\chi_E^i - \psi_0)]/(M_P^r - M_E^r)^2 = \Lambda_\chi^2(\chi_E^i, M_{E_0}, \psi_0) \quad (146)$$

The requirement of a stable solution indicates that the turning has to be oriented to reduce the angular differences relative to the line of sight. Consequently it follows, observing equations (143) and (144), as well as $\lambda^o_{M_P} < 0$ and $\lambda^o_{M_E} > 0$, that

$$\text{sign } \lambda^i_{\chi_P} = -\text{sign } u_P^i = \text{sign } (\chi_P^i - \psi) \quad (147)$$

$$\text{sign } \lambda^i_{\chi_E} = \text{sign } u_E^i = -\text{sign } (\chi_E^i - \psi_0) \quad (148)$$

Summarizing equations (141)-(148) and introducing the notion of best-sustained turning rate χ'_s, defined in equations (34) and (35), the strategy pair of the turning boundary-layer game is

$$u_P^i = \text{sat}\left(\frac{[\chi'_P(M_{P_0})]_s}{[\chi'_P(M_{P_0})]_{max}} \left\{\frac{M_{P_0}[1 - \cos(\chi_P^i - \psi_0)]}{M_P^r - M_{P_0}}\right\}^{1/2}\right) \text{sign } (\psi_0 - \chi_P^i)$$

$$= U(\chi_P^i, M_{P_0}, \psi_0) \quad (149)$$

$$u_E^i = \text{sat}\left(\frac{[\chi'_E(M_{E_0})]_s}{[\chi'_E(M_{E_0})]_{max}} \left\{\frac{M_{E_0}[1 - \cos(\chi_E^i - \psi_0)]}{M_E^r - M_{E_0}}\right\}^{1/2}\right) \text{sign } (\psi_0 - \chi_E^i)$$

$$= U(\chi_E^i, M_{E_0}, \psi_0) \quad (150)$$

3.5 Zero-Order Composite Strategies

Based on the solution of the reduced-order game and the two boundary-layer games, a uniformly valid zero-order composite strategy pair can be synthesized. This is done for a multiple time-scale differential game (refs. 2-6) by replacing, in the control strategies of the fastest (innermost) boundary layer, the initial conditions of the slower state variables by their actual current value. (This is clearly a feedback solution, where the current state is considered as a new set of initial conditions.) Such strategies guarantee that as the state approaches the equilibrium predicted by the reduced-order solution, the controls also become those required to maintain this equilibrium. Moreover, the state feedback form takes implicitly into account the eventual (small) variations of the "slow" variables in the boundary layer.

Comparing equations (139)-(144) with equations (60)-(63) indicates that the functional form of the control strategies of the exact optimal and the zero-order FSPT composite solutions is identical. The only difference is that in the FSPT solution the adjoint variables are approximated by zero-order feedback expressions.

For the sake of completeness these expressions are summarized here, denoting the variables of the zero-order composite solution by a superscript "c":

$$\lambda_{\bar{R}}^{c} = \frac{1}{(M_P^r - M_E^r)} = \text{const} \tag{151}$$

$$\lambda_{\psi}^{c} = 0 \tag{152}$$

$$\lambda_{M_P}^{c} = -\frac{M_P^r - M_P}{M_P^r - M_E^r} \cdot \frac{1}{(\bar{T}_{max} - \bar{D}_0 - \bar{D}_i)_P} = -\Lambda_M(M_P) \tag{153}$$

$$\lambda_{M_E}^{c} = \frac{M_E^r - M_E}{M_P^r - M_E^r} \cdot \frac{1}{(\bar{T}_{max} - \bar{D}_0 - D_i)_E} = \Lambda_M(M_E) \tag{154}$$

$$\lambda_{\chi_P}^{c} = \frac{-2M_P^2}{M_P^r - M_E^r} \left\{ \frac{M_P^r - M_P}{M_P} (\bar{D}_i)_P [1 - \cos(\chi_P - \psi)] \right\}^{1/2} \text{sign}(\chi_P - \psi)$$

$$= -\Lambda_\chi(M_P, \chi_P, \psi) \tag{155}$$

$$\lambda_{\chi_E}^{c} = \frac{2M_E^2}{M_P^r - M_E^r} \left\{ \frac{M_E^r - M_E}{M_E} (\bar{D}_i)_E [1 - \cos(\chi_E - \psi)] \right\}^{1/2} \text{sign}(\chi_E - \psi)$$

$$= \Lambda_\chi(M_E, \chi_E, \psi) \tag{156}$$

The uniformly valid zero-order composite control strategies are

$$\xi_P^c = \begin{cases} 1 & M_P < (M_{limit})_P \\ [(\bar{D}_0 + \bar{D}_i)/\bar{T}_{max}]_P & M_P = (M_{limit})_P \end{cases} \tag{157}$$

$$\xi_E^c = \begin{cases} 1 & M_E < (M_{limit})_E \\ [(\bar{D}_0 + \bar{D}_i)/\bar{T}_{max}]_E & M_E = (M_{limit})_E \end{cases} \tag{158}$$

$$u_P^c = \text{sat}\left(\frac{[\chi_P'(M_P)]_s}{[\chi_P'(M_P)]_{max}} \left\{ \frac{M_P[1 - \cos(\chi_P - \psi)]}{M_P^r - M_P} \right\}^{1/2} \right) \text{sign}(\psi - \chi_P)$$

$$= U(\chi_P, M_P, \psi) \tag{159}$$

$$u_E^c = \text{sat}\left(\frac{[\chi_E'(M_E)]_s}{[\chi_E'(M_E)]_{max}}\left\{\frac{M_E[1-\cos(\chi_E-\psi)]}{M_E^r - M_E}\right\}^{1/2}\right)\text{sign}\ (\psi - \chi_E)$$

$$= U(\chi_E, M_E, \psi) \tag{160}$$

The following qualitative comments can be made about these zero-order strategies.

1. Full thrust ($\xi = 1$) is an inherent feature of the FSPT model selected for the analysis (if the placard-speed limit is not reached). It is a direct consequence of the assumption that speed variations are slower than turning dynamics. In most cases this assumption is verified by the solution itself (see section 6.1). However, "exact" numerical solutions reveal that for some extreme set of initial conditions, such as combination of very high speed and large angular disadvantage ($\chi - \psi \approx +\pi$) zero thrust is optimal. To approximate such situations a different FSPT model, described in reference 4, is needed.

2. The commanded unconstrained (suboptimal) turning rate can be expressed by

$$|(\chi')^c| = \chi_s'(M)\left\{\frac{M[1-\cos(\chi-\psi)]}{M^r - M}\right\}^{1/2} \tag{161}$$

Relating the commanded turning rate to the best sustained turning performance indicates the compromise made in the optimization process between fast turning and acceleration, both required for successful interception.

3. The function $(1-\cos\beta)^{1/2}$ depicted in figure 3 is of particular interest. For small values of β it is almost linear. This indicates that for small deviations from the required heading, the optimal strategy reduces to a proportional control with a gain of $\{\chi_s'[M/(M^r - M)]^{1/2}\}$.

4. The speed-dependent gain factor provides an additional insight. It indicates that if the current speed is near to its maximum value, that is, if there is little need for acceleration, a harder turn can be made. Conversely, if $(M^r - M)$ is large, it is better not to lose speed in a sharp turn but to use excess thrust for acceleration.

5. It can be shown that the gain factor is monotonically increasing in the vicinity of the maximum speed for level flight, as determined by thrust/drag equilibrium, and that it approaches a finite limit at this speed:

$$\lim_{M \to \tilde{M}} \chi_s'[M/(\tilde{M} - M)]^{1/2} = \left[(-1/\tilde{M})\cdot\frac{\partial}{\partial M}\frac{(\bar{T}_{max} - \bar{D}_0)}{\bar{D}_i}\Big|_{\tilde{M}}\right]^{1/2} > 0 \tag{162}$$

6. If the maximum speed is placard-limited, that is, if

$$M_{max} = M_{limit} < \tilde{M} \triangleq \arg\left\{\bar{T}_{max} = \bar{D}_0 + \bar{D}_i\right\} \tag{163}$$

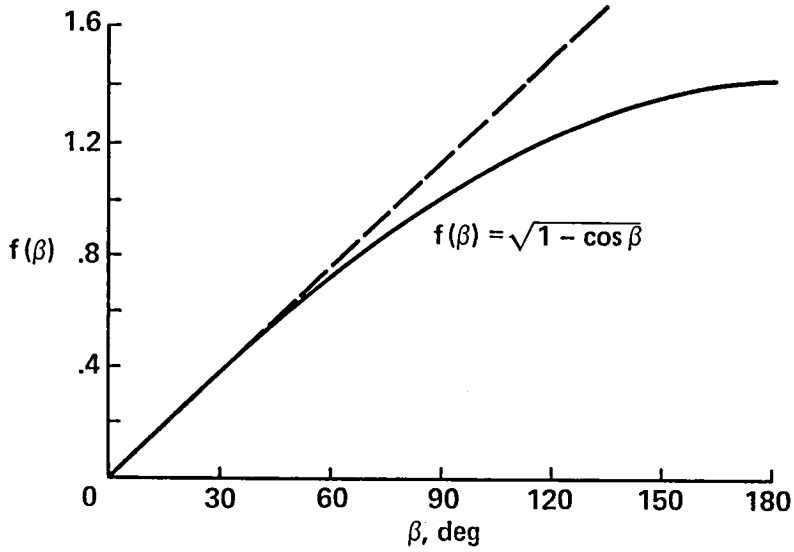

Figure 3.- The function $(1 - \cos \beta)^{1/2}$.

the gain becomes infinite. It means that if this limiting speed is reached before the angular deviation becomes zero, the remaining error has to be corrected using maximum turning rate. The same phenomenon was observed in the exact numerical solution of similar problems (refs. 20, 21).

7. The feedback expressions of equations (157)-(160) are easily applicable to an onboard implementation. They require measurements that are accessible in most airplanes (as speed, heading, and line of sight direction). No range measurements or estimation of opponent state variables are needed. Such a feedback chart, superposable on figure 2, is depicted in figure 4.

The zero-order composite strategies of equations (157)-(160) were implemented for a digital simulation on the IBM 360/67 at Ames Research Center, using CSMP III language.

Results of this digital simulation, using the zero-order FSPT composite strategies, were compared with the set of existing exact open-loop solutions described in the next section.

4. DESCRIPTION OF THE OPEN-LOOP OPTIMAL SOLUTION

The original horizontal interception game formulated in section 2 is of six dimensions. It has been well known that since aircraft dynamics is independent of the horizontal flight direction, the order of the system can be reduced to five by using relative angular coordinates. In references 17-19 directions are measured relative to the line of sight, and the final line of sight direction is used as reference. In this particular coordinate system, the necessary conditions of game optimality are decoupled into two one-sided optimal control problems, which can be solved independently. This approach enables one to generate extremal trajectories for each airplane, independently of its role, of the position of its opponent, and of the capture conditions. Such open-loop trajectories are obtained by simultaneous retrograde integration of the state and adjoint equations with a given set of end conditions. For a game solution, two respective trajectories can be superposed, separated by the distance of capture measured along the final line of sight, if the conditions for capture are satisfied. The construction of an individual extremal trajectory is essentially identical to the method proposed and explored for the solution of a time-optimal turn to a point with unspecified final direction (refs. 20, 21).

In order to obtain the open-loop optimal trajectory for any given initial condition, a systematical search has to be carried out in the parameter space of the terminal conditions (terminal speed, direction, and time). This effort and its further implementation is reported in reference 22. Because of the excessive numbers of computations required to match a given set of initial conditions, it was decided that only existing extremal trajectories would be used for comparison. Any point along such an extremal can be considered as an initial point of some engagement.

The open-loop extremals of reference 22 were calculated in a set of "normalized" coordinates, different from the one introduced in section 2 and used in the sequel to derive the FSPT approximation. Time was not normalized, but distances were divided by the speed of sound in order to be consistent with the representation of velocities by Mach numbers. Moreover, relative geometry was computed in Cartesian coordinates.

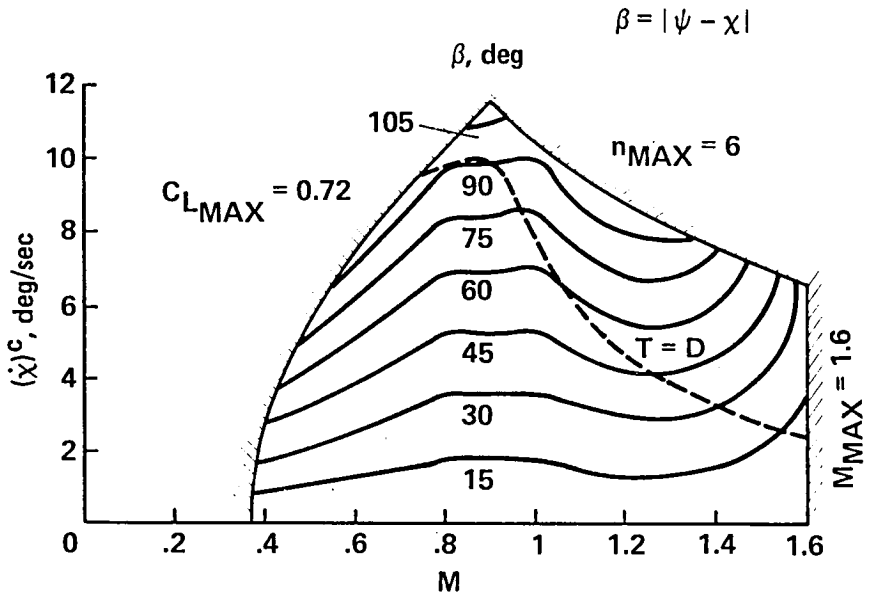

Figure 4.- Feedback chart for suboptimal turning.

For the sake of convenience in making the comparison, the same variables were used in the computer program of the digital simulation, implementing the zero-order FSPT feedback control strategies (see appendix).

The aircraft model used in the simulation (identical to the one used in reference 22) and the criteria for selecting examples for comparison are discussed in the next section.

5. AIRCRAFT MODEL AND CONDITIONS OF COMPARISON

In order to be consistent with the limitations of using only existing results, all computations were performed for an altitude of 20,000 ft, implying a = 316.1 m/sec and $\rho/\rho_0 = 0.5326$. For the same reason the same aircraft model (an early version of the F4-B, used first by Bryson et al. (ref. 23) and later by Bryson and Parson (refs. 20, 21) served both as pursuer and evader. General aircraft information is summarized in table 1, and the aerodynamic and propulsion data at h = 20,000 ft are given in table 2 for Mach numbers from 0.6-1.6.

TABLE 1.- GENERAL AIRCRAFT INFORMATION

Weight	W = 25,000 lb (15,875 kg)
Wing area	S = 530 ft^2 (49.23 m^2)
Wing loading	(W/S) = 66 lb/ft^2 (322.4 kg/m^2)
Maximum Mach number (at 20,000-ft)	M_{max} = 1.6
Maximum load factor	n_{max} = 6.0
Maximum usable lift coefficient	$C_{L_{max}}$ = 0.72

TABLE 2.- AERODYNAMIC AND PROPULSION DATA

Parameter	Mach number					
	0.6	0.8	1.0	1.2	1.4	1.6
C_{Do}	0.013	0.013	0.014	0.041	0.039	0.036
K	0.157	0.157	0.180	0.247	0.296	0.343
T_{max}/W	0.491	0.566	0.666	0.780	0.903	1.02

Note: Altitude = 20,000 ft; speed of sound = 316.1 m/sec; density ratio = 0.5326.

Since the singular-perturbation methods assume a time-scale separation between trajectory and airplane dynamics, only open-loop extremals of relatively long duration can be considered as candidates for meaningful comparison. As a reasonable limit, $t_f \geq 50$ sec was selected. Respective points on any two extremals can be candidates for initial conditions if the capturability condition

$$M_P(t_f) > M_E(t_f) \tag{164}$$

is satisfied. The terminal and initial conditions of the available extremal trajectories are summarized in table 3. For all cases, the optimal throttle setting is maximal ($\xi^* = 1$), consistent with the FSPT solution described in section 2.

TABLE 3.- END CONDITIONS OF EXTREMAL TRAJECTORIES

Trajectory number	M_f	M_0	t_f^*, sec	χ_0, rad	χ_f, rad	$\hat{X}_f$[a]	$\hat{Y}_f$[a]
I	1.5	1.238	97.1	1.330	1.7×10^{-7}	126.68	13.21
II	1.4	1.174	97.1	3.077	1.7×10^{-7}	97.30	16.48
III	1.377	1.2	50.0	9.550	1.2×10^{-5}	63.78	4.83
IV	1.272	1.2	50.0	2.280	3.5×10^{-5}	47.11	14.20
V	1.222	0.9	60.0	2.917	5.2×10^{-6}	49.05	11.31

[a]One unit is 316.1 m.

For the selected initial condition pairs listed in table 4, the best turning radii of the airplanes are computed. For any pair of initial conditions, the value of $(X_0 - X_f)$, computed from the individual trajectories as

$$X_0 - X_f = X_P(t_f) - X_E(t_f) \tag{165}$$

was kept constant. By varying X_f (the capture range), a large set of differential games, with different initial ranges, can be formulated.

For the constant-speed model of reference 2, it was shown that the small parameter, characterizing the time-scale separation between trajectory and aircraft dynamics, is the ratio of the minimum turning radius of the airplane r to the initial distance of separation

$$\varepsilon_g \triangleq r/R_0 \tag{166}$$

Though in the variable-speed case the technique of "forced" singular perturbations (an artificial insertion of a perturbation parameter $\varepsilon = 1$) was used, such a ratio still provides a measure of the time-scale separation. The validity of the singular-perturbation approach depends on the value of this parameter. For each pair of trajectories the distance of capture selected in such a way that ε_g be in the range of $0.1 < \varepsilon_g < 0.25$. For sake of uniformity the turning radius of the pursuer was used as reference.

TABLE 4.- SELECTED INITIAL CONDITIONS FOR COMPARISON

Example number	Trajectory number		M_{P0}	χ_{P0}, rad	$\hat{r}_p^a$	M_{E0}	χ_{E0}, rad	$\hat{r}_E^a$	$\hat{X}_0-\hat{R}_f^a$	t_f^*, sec
	P	E								
1.	I	II	1.238	1.33	8.35	1.174	3.077	7.51	29.38	97.1
2.	III	IV	1.20	0.55	7.84	1.20	2.280	7.84	16.67	50.0
3.	III	V	1.20	0.55	7.84	0.822	0.960	4.43	21.23	50.0
4.	II	V	1.167	0.03	7.42	0.90	2.917	4.41	28.62	60.0

[a]One unit = 316.1 m.

In the next section selected results are presented in detail and analyzed.

6. COMPARISON OF RESULTS

6.1 Qualitative Comparison

Analysis of the open-loop extremals allows certain qualitative conclusions to be drawn. The very nature of the independent extremals exhibits a strong similarity with the zero-order FSPT solution. As was pointed out in section 3, the forced-singular-perturbation technique leads to a decoupling of the original differential game to a "simple pursuit" game and two independent sets of multiple time-scale control problems optimizing an accelerating turn to the instantaneous line of sight. The exact open-loop-optimal solution does the same, but relative to the final direction of the line of sight. If time-scale separation between airplane turning dynamics and variations of the relative geometry is a valid assumption, then the current direction of the line of sight presents a good approximation to its final direction. In such a case, it can be expected that the accuracy of the zero-order feedback approximation would be satisfactory.

The control strategies obtained by the two different methods are vey similar. Both require full thrust for time-optimal interception if the maximum speed limit is not attained. (In the examples used, the speed limits were never reached.) The turning strategies are characterized by a gradually decreasing rate of turn, as the flight direction asymptotically reaches the required value. The only difference between the exact and the zero-order solution is the reference direction. The larger the difference between the instantaneous and final directions of the line of sight, the worse the accuracy of the FSPT approximation.

These qualitative differences are shown by comparing the time histories of the control and state variables of the pursuer and the evader for a particular example. The initial conditions for this example are depicted in figure 5. In order to obtain observable differences, a relative high value of the geometric perturbation parameter, $\epsilon_g = 0.25$, was selected. In figures 6 and 7 the load factor time histories of the evader and the pursuer are shown. Figures 8 and 9 depict the time histories of the respective flight directions; the line of sight direction is also shown in these figures.

It can be observed from these figures that the initial load-factor time-histories are very similar. The evader, using the FSPT strategy, reaches the actual line of sight very nearly at the same time as the open loop optimal trajectory closely approaches the final (reference) direction. Its FSPT turning strategy can, therefore, be considered as close to optimal. One cannot say the same about the pursuer. Since the initial conditions of the pursuer are more favorable than those of the evader, the pursuer can reach the line of sight in a shorter time. Because the evader has not yet completed its turn, the line of sight continues to rotate. Consequently, the pursuer, using FSPT control strategy, has made an unnecessary turn (an overshoot) which has to be corrected later. As a result, it can be expected that the capture time of the suboptimal FSPT game will be longer than the optimal one.

In figures 10 and 11, Mach number time-histories of the evader and the pursuer are shown, respectively; in figures 12 and 13 the initial turning geometry of the airplanes is depicted. It can be observed in figure 11 that because of the unnecessary turn, the velocity of the pursuer, using FSPT strategy, is slightly lower than the velocity shown by the results of the optimal solution, as it has been expected. This is in addition to the geometrical disadvantage shown in figure 13. Indeed, for this example, the time of capture predicted by the FSPT approximation is about 6.5% higher than the optimal value of 97.1 sec.

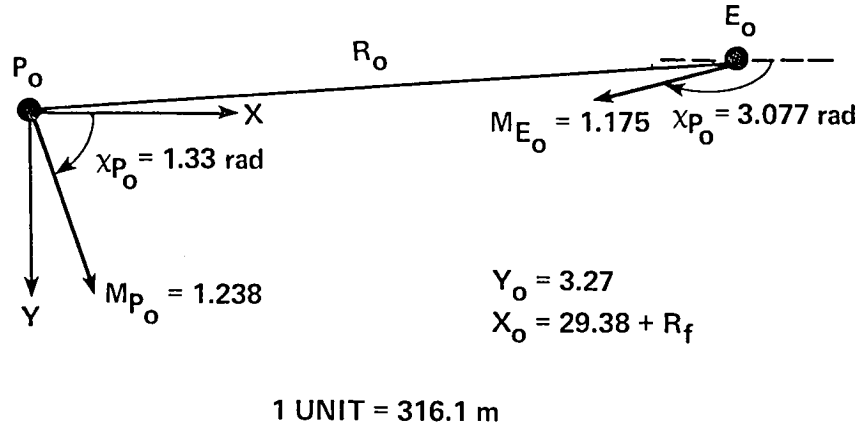

Figure 5.- Initial conditions for example No. 1.

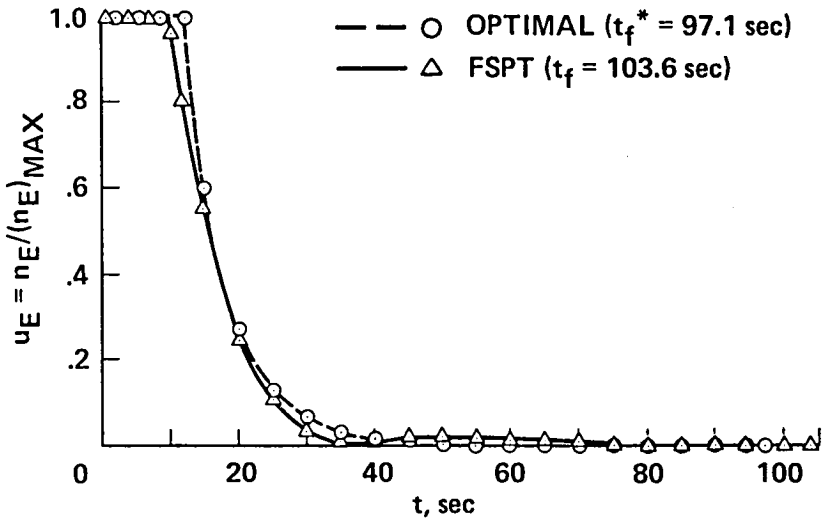

Figure 6.- Evader's load factor time-history.

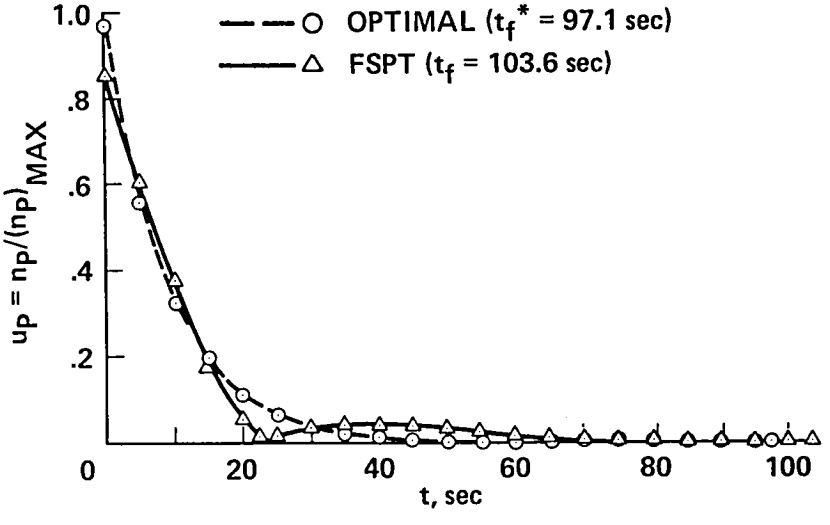

Figure 7.- Pursuer's load factor time-history.

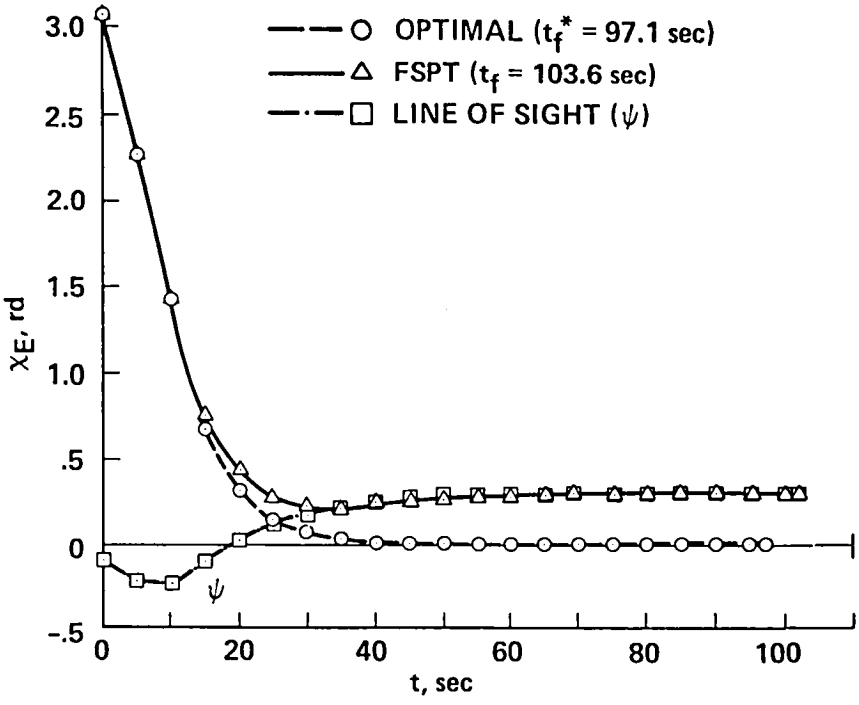

Figure 8.- Evader's turning time-history.

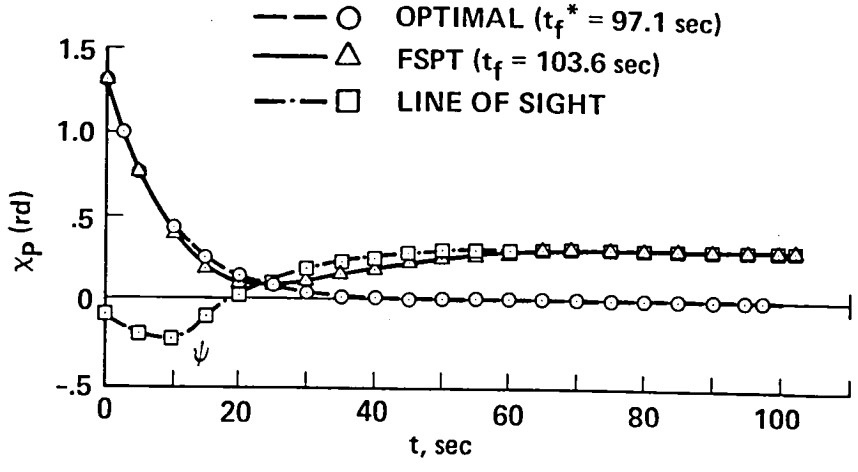

Figure 9.- Pursuer's turning time-history.

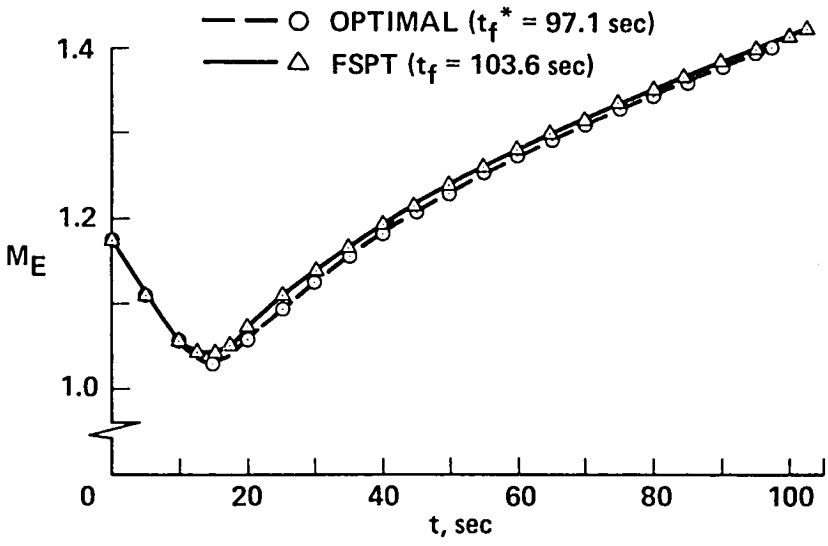

Figure 10.- Evader's Mach number time-history.

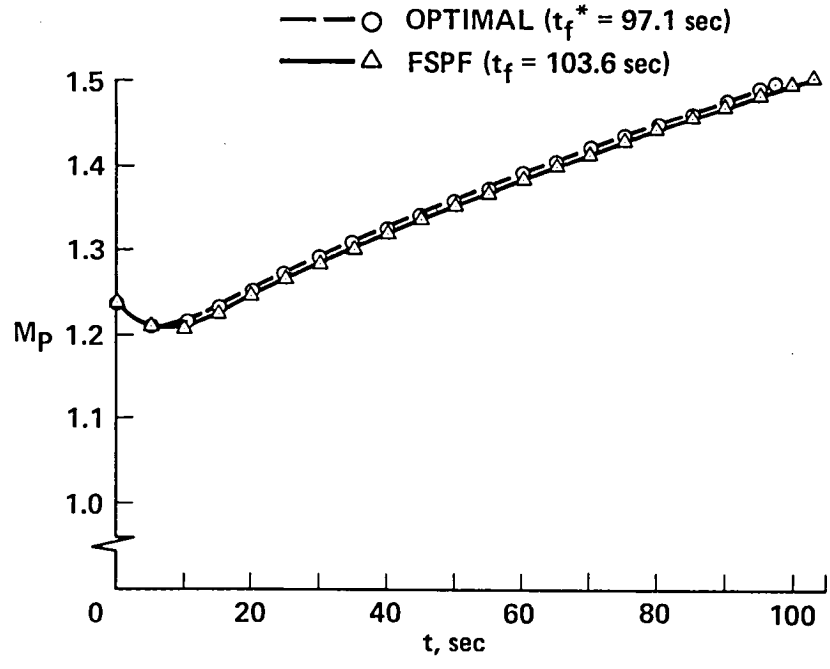

Figure 11.- Pursuer's Mach number time-history.

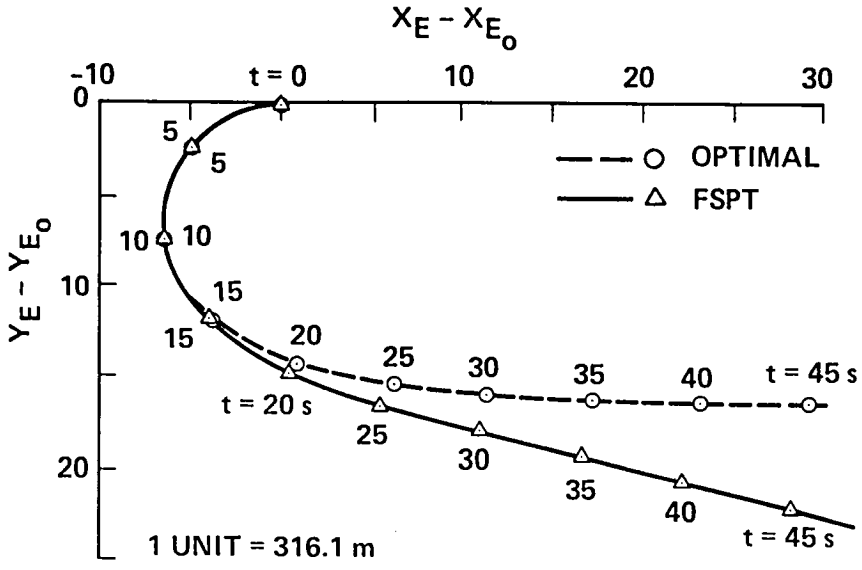

Figure 12.- Evader's initial turning geometry.

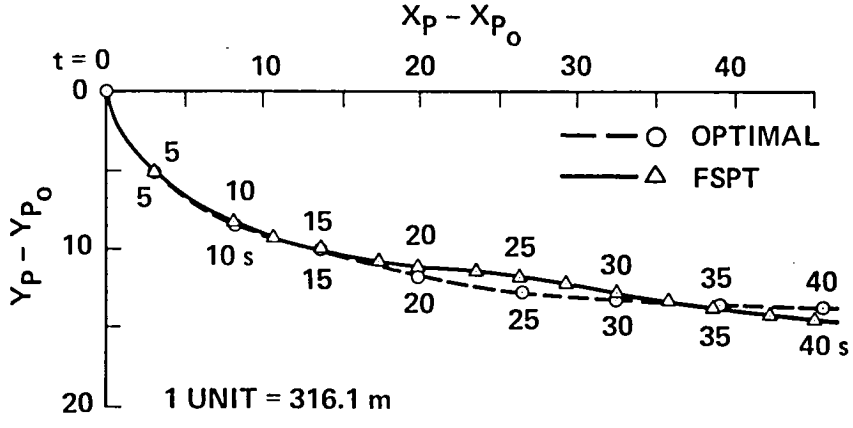

Figure 13.- Pursuer's initial turning geometry.

6.2 Quantitative Comparison of Payoff Accuracy

The purpose of such quantitative comparison is to determine the range of parameters or the domain of initial conditions for which the accuracy of the zero-order FSPT feedback solution is satisfactory. If this domain contains a region of practical interest, then the approximation can be considered useful.

The example analyzed in detail in the previous subsection and depicted in figures 5-13 was recomputed with different initial and terminal ranges, keeping the relative "distance-to-close" constant. In figure 14 the relative payoff accuracy of the zero-order FSPT feedback approximation, defined as

$$\frac{\Delta t_f}{t_f^*} \triangleq \frac{t_f - t_f^*}{t_f^*} \tag{167}$$

is plotted versus the inverse of the geometrical perturbation parameter of the pursuer, defined by

$$\frac{1}{(\varepsilon_g)_p} = \frac{R_0}{r_p(M_{P_0})} \tag{168}$$

as a ratio of the initial range divided by the pursuer's best turning radius at its initial Mach number, M_{P_0}.

In figures 15-17, similar results of three additional examples, generated based on the available extremal trajectories listed in table 3, are plotted. The initial game conditions are summarized for comparison in table 4. These examples are characterized by the fact that the final Mach number of the extremal trajectory is very different from the maximum value. Consequently, the assumption made in the FSPT solution that $M^r = M_{max}$ is not validated. This discrepancy can result in control strategies that deviate strongly from the optimal one. In the present examples this difficulty was overcome by adjusting the value of M^r in the respective control strategies by a min-max (max-min) parameter optimization technique. The values of the adjusted parameters M_P^r, M_E^r are noted in the respective figures. All four of the last figures (figs. 14-17) show that the accuracy level of 1%, which is highly satisfactory for all practical purposes, is satisfied if ε_g is of the order of 1/8 or less. Since in all the available examples the pursuer had less of a turning requirement, its suboptimal strategy deviates from the optimal more than that of the evader. Consequently, the capture time obtained by the FSPT strategy pair is always higher than the optimal.

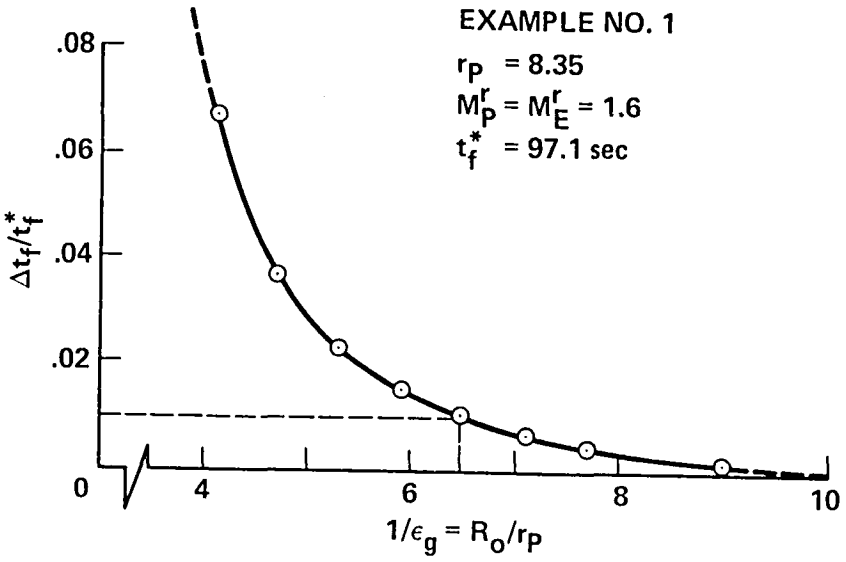

Figure 14.- Payoff accuracy of the zero-order FSPT solution: example No. 1.

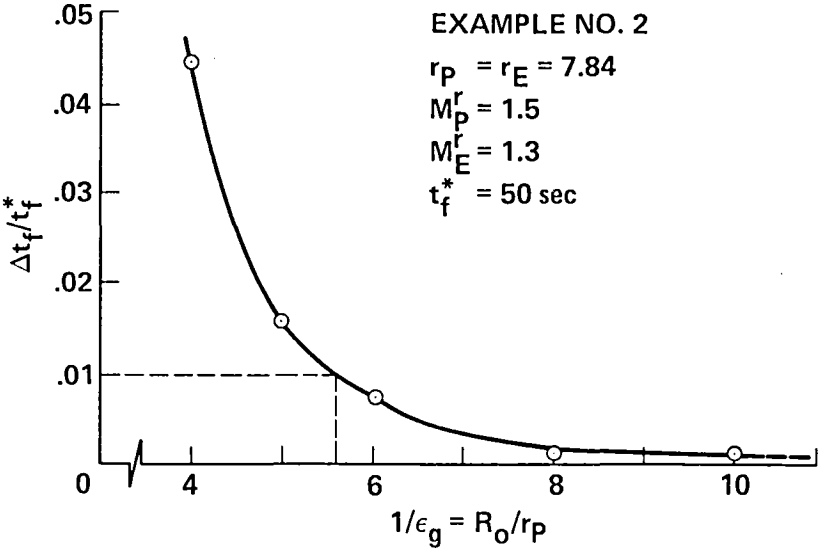

Figure 15.- Payoff accuracy of the zero-order FSPT solution: example No. 2.

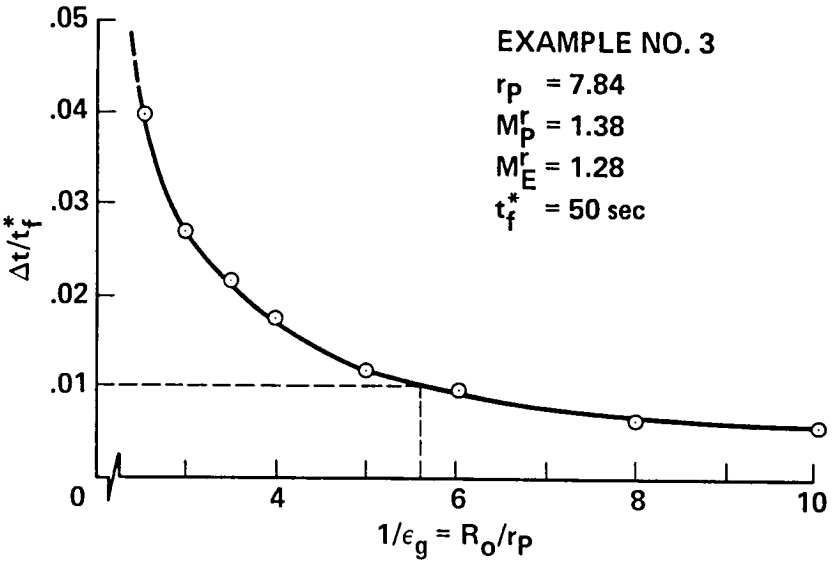

Figure 16.- Payoff accuracy of the zero-order FSPT solution: example No. 3.

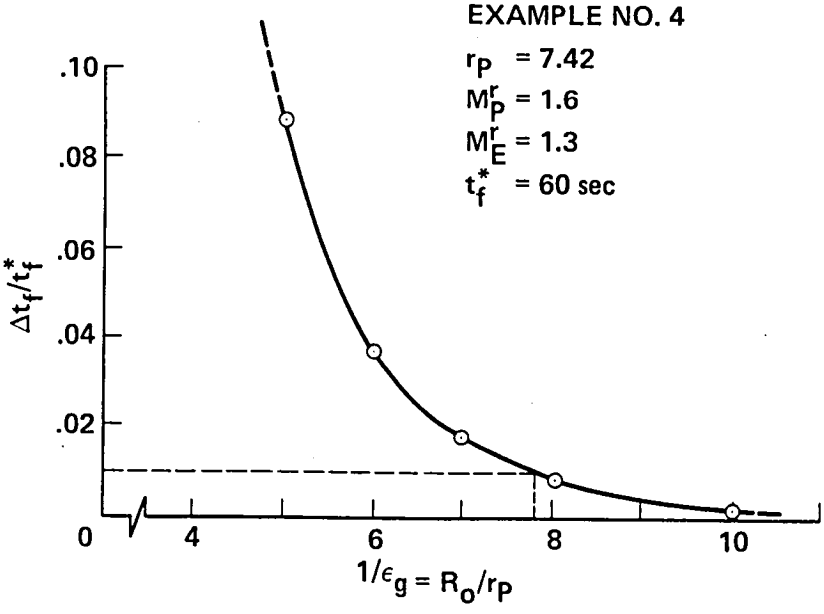

Figure 17.- Payoff accuracy of the zero-order FSPT solution: example No. 4.

7. CONCLUSIONS

Results of the comparison, presented and discussed in this report, lead to the conclusion that the method of forced singular perturbation provides a valid mathematical tool for analyzing medium- and longer-range pursuit-evasion engagements. The demonstrated accuracy of the FSPT approximation is very encouraging. Taking 1% accuracy as a measure of practical usefulness, it follows that the method is applicable to medium-range air-to-air combat (as defined in the Introduction).

The turning radius of an airplane at speeds higher than the corner velocity is determined by equation (31). This expression gives (approximately), for an example of a 6-g-limit load factor and an altitude of 20,000 ft,

$$r \approx 1.5\ M^2 \text{ (km)} \tag{169}$$

The maximum firing range of advanced air-to-air missiles in a tail-chase situation (being of the order of 4-8 km, depending on the altitude) is typically larger than the aircraft turning radius. As a consequence, side-stepping maneuvers, which would have invalidated the presented FSPT approach, are not optimal. Results of the present comparison show that the required accuracy of 1% is guaranteed by $\epsilon_g \leq 0.125$ (see figs. 14-17).

The domain of initial ranges for valid zero-order FSPT analysis can be thus determined by

$$R_0 \geq 12\ (M_0)_P^2 \text{ (km)} \tag{170}$$

Such an inequality is definitely compatible with medium-range interceptions of a real operational scenario.

It should be noted, however, that the validation of the FSPT approximation presented in this report is by no means comprehensive. Because of inherent limitations, detailed in section 5, only horizontal engagements were analyzed, only a single airplane model was investigated, and the set of initial conditions was limited. Moreover, the necessity for eventual parameter adjustment requires further investigation.

Nevertheless, the accuracy of the FSPT method was demonstrated recently in an independent study of a closely related problem (ref. 24). In that work, the three-dimensional medium-range interception, formulated as a one-sided optimal control problem, was analyzed. Such a demonstration could not have been performed for a differential game formulation because of the lack of an operating numerical technique, as explained in the Introduction. The currently presented comparison, together with the results of reference 24 provides a sufficient basis to encourage further investigations applying FSPT to air-combat-motivated differential game analysis.

The attractiveness of the FSPT approach is that it provides a feedback control strategy for onboard applications. Because of the simplicity of the implementation, it can be incorporated in any future integrated fire and flight control system with virtually no additional effort or cost.

REFERENCES

1. Ardema, M. D.: Air-to-Air Combat Analysis: Review of Differential-Gaming Approaches. Joint Automatic Control Conference, Charlottesville, Va., June 17-19, 1981.

2. Farber, N.; and Shinar, J.: Approximate Solution of Singularly Perturbed Nonlinear Pursuit-Evasion Games. JOTA, vol. 32, no. 1, Sept. 1980, pp. 39-73.

3. Farber, N.; and Shinar, J.: An Approximate Feedback Solution of a Variable Speed Nonlinear Pursuit-Evasion Game between Two Airplanes in a Horizontal Plane. AIAA Paper 80-1597, 7th Atmospheric Flight Mechanics Conference, Danvers, Mass., Aug. 1980, pp. 337-347.

4. Farber, N.; and Shinar, J.: A Variable Modelling Approach for Singularly Perturbed Pursuit-Evasion Problems. TAE Report No. 433, Technion, Israel Inst. of Technology, Haifa, Israel (presented at the 23rd Israel Annual Conference on Aviation and Astronautics, Feb. 11-12, 1981).

5. Shinar, J.: Solution Techniques for Realistic Pursuit-Evasion Games. Control and Dynamic Systems, C. T. Leondes, ed., vol. 17, Academic Press, N.Y., 1981, pp. 64-125.

6. Farber, N.: Improved Dynamic Models for Air Combat Analysis. D. Sc. Dissertation, Technion, Israel Inst. of Technology, Haifa, Israel, May 1981.

7. Roberts, D. A.; and Montgomery, R. C.: Development and Application of a Gradient Method for Solving Differential Games. NASA TN D-6502, 1971.

8. Leatham, A. L.: A Neighboring Optimal Method to Solve Differential Games Involving Realistic Aerodynamic Vehicle Models. AFFDL-TM-73-56-FXG, Air Force Flight Dynamics Laboratory, Wright-Patterson AFB, Ohio, 1973.

9. Lynch, U.H.D.: The Simultaneous Minmax Gradient Technique for Solving the Air-to-Air Combat Differential Game. AFFDL TM-73-57-FXG, Air Force Flight Dynamics Laboratory, Wright-Patterson AFB, Ohio, 1973.

10. Anderson, G. M.: A Near Optimal Closed Loop Solution Method for Non-Singular Zero-Sum Differential Games. JOTA, vol. 13, no. 3, 1974.

11. Neeland, R. P.: The Numerical Solution of a Nonlinear, Control Constrained, Air-to-Air Combat Differential Game. Ph.D. Dissertation, U. of California, Los Angeles, 1974.

12. Miller, L. E.: Differential Game Computer Program. AFFDL TM 75-66-FXG, Air Force Flight Dynamics Laboratory, Wright-Patterson AFB, Ohio, 1977.

13. Järmark, B.: Convergence Control in Differential Dynamic Programming Applied to Air-to-Air Combat. AIAA J., vol. 14, no. 1, Jan. 1976.

14. Enjalbert, B.: Résolution Numériques pour les problèmes de jeux differentiels. Thèse de 3 ème cycle, Université de Paris, 1979.

15. Blaquiere, A.; Gerard, F.; and Leitmann, G.: Quantitative and Qualitative Games. Academic Press, New York, 1969.

16. Stall, M.; and Enjalbert, B: Comparaison de solutions en boucle ouverte et en boucle fermée d'ordre zéro d'une problème de combat aérien bidimensionnel avec critère de distance. Division d'Etudes Avancés, Avions Marcel Dassoult-Breguet Aviation, St. Claud, France (an internal technical note), May 1981.

17. Rajan, N.; Prashad, U. R.; and Rao, N. J.: Pursuit-Evasion of Two Aircraft in a Horizontal Plane. J. G&C, vol. 3, no. 3, May-June 1980, pp. 261-267.

18. Prashad, U. R.; Rajan, N.; and Rao, N. J.: Planar Pursuit-Evasion with Variable Speeds. Part 1. JOTA, vol. 33, no. 3, Mar. 1981, pp. 401-418.

19. Rajan, N.; Prashad, U. R.; and Rao, N. J.: Planar Pursuit-Evasion with Variable Speeds. Part 2. JOTA, vol. 33, no. 3, Mar. 1981, pp. 419-432.

20. Bryson, A. E., Jr.; and Parsons, M. G.: Constant Altitude Minimum-Time Turns to a Line and to a Point for a Supersonic Aircraft with a Constraint on Maximum Velocity. Stanford U. SUDAAR No. 437, Stanford, Calif., Nov. 1971.

21. Parsons, M. G.: Three-Dimensional, Minimum Time Turns to a Point and onto a Line for a Supersonic Aircraft with a Mach Number Constraint. Ph.D. Dissertation, Stanford U., Aug. 1972.

22. Rajan, N.; and Ardema, M. D.: Minimum Time Interception of a Target Moving in a Horizontal Plane. Submitted for AIAA Guidance and Control Conference, 1982.

23. Bryson, A. E., Jr.; Desai, M. N.; and Hoffman, W. L.: The Energy State Approximation in Performance Optimization of Supersonic Aircraft. J. Aircraft. vol. 6, no. 6, Nov.-Dec. 1969, pp. 481-487.

24. Shinar, J.; Negrin, M.; Well, K. H.; and Berger, E.: Comparison between the Exact and an Approximate Feedback Solution for Medium Range Interception Problems. Joint Automatic Control Conference, Charlottesville, Va., June 17-19, 1981.

1. Report No.	2. Government Accession No.	3. Recipient's Catalog No.
NASA TM-84237		

4. Title and Subtitle	5. Report Date
VALIDATION OF ZERO-ORDER FEEDBACK STRATEGIES FOR MEDIUM RANGE AIR-TO-AIR INTERCEPTION IN A HORIZONTAL PLANE	6. Performing Organization Code

7. Author(s)	8. Performing Organization Report No.
Josef Shinar	A-8895
	10. Work Unit No. T-5259

9. Performing Organization Name and Address	11. Contract or Grant No.
NASA Ames Research Center Moffett Field, Calif. 94035	

12. Sponsoring Agency Name and Address	13. Type of Report and Period Covered
National Aeronautics and Space Administration Washington, D.C. 20546	Technical Memorandum
	14. Sponsoring Agency Code 307-01-00

15. Supplementary Notes

Point of Contact: Josef Shinar, Ames Research Center, MS 210-9, Moffett Field, Calif. 94035 (415) 965-5431 or FTS 448-5431.

16. Abstract

A zero-order feedback solution of a variable-speed interception game between two aircraft in the horizontal plane, obtained by using the method of forced singular perturbations (FSP), is compared with the exact open-loop solution. The comparison indicates that for initial distances of separation larger than 8 turning radii of the evader, the accuracy of the feedback approximation is better than 1%. The result validates the zero-order FSP approximation for medium-range air-combat analysis. This feedback solution is a very attractive candidate for airborne implementation.

17. Key Words (Suggested by Author(s))	18. Distribution Statement
Air combat analysis Pursuit-evasion games Singular perturbations Feedback strategies	Unlimited Subject Category — 05

19. Security Classif. (of this report)	20. Security Classif. (of this page)	21. No. of Pages	22. Price*
Unclassified	Unclassified	48	A03

*For sale by the National Technical Information Service, Springfield, Virginia 22161